Enhancement of Proximity Induced Superconductivity in Planar Germanium

Kushagra Aggarwal,[1,*] Andrea Hofmann,[1] Daniel Jirovec,[1] Ivan Prieto,[1] Amir Sammak,[2] Marc Botifoll,[3] Sara Martí-Sánchez,[3] Menno Veldhorst,[4] Jordi Arbiol,[3,5] Giordano Scappucci,[4] and Georgios Katsaros[1,†]

[1] *Institute of Science and Technology Austria, Am Campus 1, 3400 Klosterneuburg, Austria*
[2] *QuTech and Netherlands Organisation for Applied Scientific Research (TNO), Stieltjesweg 1, 2628 CK Delft, The Netherlands*
[3] *Catalan Institute of Nanoscience and Nanotechnology (ICN2), CSIC and BIST, Campus UAB, 08193 Bellaterra, Barcelona, Catalonia, Spain*
[4] *QuTech and Kavli Institute of Nanoscience, Delft University of Technology, Lorentzweg 1, 2628 CJ Delft, The Netherlands*
[5] *ICREA, Pg. Lluís Companys 23, 08010 Barcelona, Catalonia, Spain*

(Dated: December 2, 2020)

Holes in planar Ge have high mobilities, strong spin-orbit interaction and electrically tunable g-factors, and are therefore emerging as a promising candidate for hybrid superconductor-semiconductor devices. This is further motivated by the observation of supercurrent transport in planar Ge Josephson Field effect transistors (JoFETs). A key challenge towards hybrid germanium quantum technology is the design of high quality interfaces and superconducting contacts that are robust against magnetic fields. By combining the assets of Al, which has a long superconducting coherence, and Nb, which has a significant superconducting gap, we form low-disordered JoFETs with large $I_C R_N$ products that are capable of withstanding high magnetic fields. We furthermore demonstrate the ability of phase-biasing individual JoFETs opening up an avenue to explore topological superconductivity in planar Ge. The persistence of superconductivity in the reported hybrid devices beyond 1.8 T paves the way towards integrating spin qubits and proximity-induced superconductivity on the same chip.

I. INTRODUCTION

While semiconducting and superconducting qubits have been used to demonstrate control over quantum information, decoherence remains a crucial challenge towards building a large-scale, universal quantum processor. This has prompted intense efforts for engineering Majorana Zero Modes (MZMs) in superconductor-semiconductor (S-Sm) devices, which are predicted to encode quantum information non-locally resulting in protection against decoherence [1, 2]. In addition, hybrid devices have attracted significant interest over the past few years due to the ensuing Andreev physics and their potential towards building electrically tunable Josepshon junction (JJ) based qubits and long range coupling of spin qubits [3–12].

The recent advancements in material science and fabrication has lead to a resurgence of interest in Ge [3, 5, 13, 14]. Ge offers several key physical properties such as inherent spin-orbit coupling, low hyperfine interaction and electrically tunable g-factors due to the carrier states originating from the valence band. In particular, the prospect of compatibility with existing Si foundry makes planar Ge a favourable platform for future quantum technologies [15]. Indeed, the recent results with spin qubits and hybrid S-Sm devices underline its potential [16–20].

So far Al remains the foremost choice as a superconductor in hybrid S-Sm devices due to its large superconducting coherence length. However, its limited magnetic field resilience acts as a deterrent for exploring exotic condensed matter phases. Among other common choices, Nb and NbTiN offer a higher superconducting gap and magnetic resilience, but forming high quality interfaces with semiconductors remains a challenge. Here, we demonstrate induced superconductivity in Ge quantum wells (QWs) overcoming the main challenges of low transparency S-Sm interfaces and limited magnetic field resilience. Al forms high transparency and low disorder interfaces with the Ge QW. The thin Al layer is directly contacted by Nb, resulting in an increase in the superconducting gap of Al. We markedly see a higher critical magnetic field and critical temperature in comparison to solely Al based devices. Moreover, we show superconducting phase control over our junctions which allows to devise Φ_0 junctions and explore low magnetic field topological superconductivity [21]. The characterization of different energy scales will enable the design of future hybrid devices for quantum information processing in planar Ge.

II. RESULTS

A. Josephson Field Effect Transistors

A Josephson Field Effect Transistor (JoFET), formed by sandwiching a semiconductor between two superconductors, allows to observe phase coherent Andreev transport reflecting the quality of the S-Sm interface and the underlying transport in the semiconductor. We fabricate JoFETs with a strained Ge/SiGe heterostructure as a semiconducting weak-link. Densities of $6 \times 10^{11}\,\mathrm{c\,m^{-2}}$ and mobilities up to $5 \times 10^5\,\mathrm{c\,m^2/V\,s}$, leading to mean

*Electronic address: kushagra.aggarwal@ist.ac.at
†Electronic address: georgios.katsaros@ist.ac.at

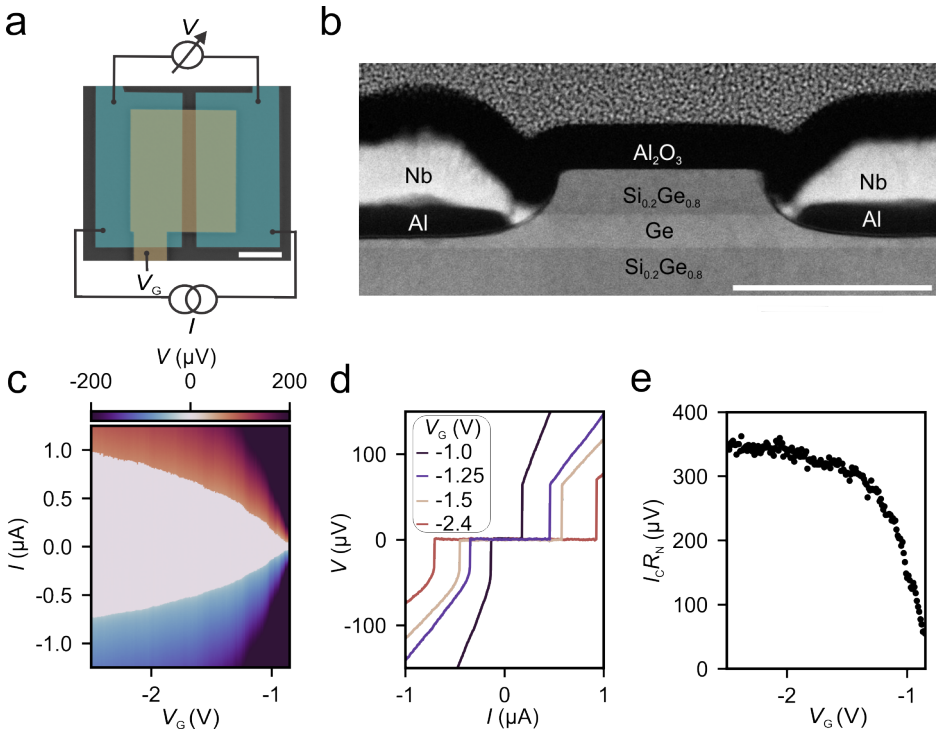

FIG. 1: **(a)** False-colored SEM of a Ge JoFET with a top gate (yellow) accumulating a 2DHG between the two superconducting electrodes (blue). The scale bar is 500 nm. **(b)** HAADF-STEM image of the cross-section of the JoFET with the Al layer directly contacting the Ge QW. The scale bar is 100 nm. **(c)** V measured across the JoFET versus V_G and I. The device can be fully switched off at more positive voltages. **(d)** V versus I traces, extracted from **(c)**, highlighting the switching current at different V_G. **(e)** Dependence of the $I_C R_N$ product on V_G as extracted from **(c)**.

free paths l_e up to 6 µm, are routinely achieved in a nominally identical wafer [22]. Figure 1a shows the false colored scanning electron microscope (SEM) image of a JoFET with the superconducting electrodes separated by a distance $L = 150$ nm and a top gate electrically isolated from the superconducting contacts by aluminium oxide. Further details on the fabrication of the devices can be found in the methods. Figure 1b shows the cross-section High-Angle Annular Dark Field Scanning Transmission Electron Microscopy (HAADF-STEM) image of an identical JoFET where the Ge QW between two SiGe spacers is directly contacted by a thin film of Al to form a low-disorder and high transparency interface. Al itself is contacted by Nb resulting in a hybrid S'-S-Sm junction. The etching procedure produces a concave interface resulting in a larger segment of semiconducting weak-link than lithographically defined, potentially affecting the transport. A detailed overview of the HAADF-STEM and STEM- Electron Energy-Loss Spectroscopy (EELS) analyses are presented in the Supplementary Material.

The JoFETs are measured in a four-terminal current-biased configuration at a base temperature of 20 mK. A top gate is used to tune the density of the underlying two-dimensional hole gas (2DHG) and we observe a gate voltage dependent switching current I_S of about 1 µA at a negative gate voltage of -2.5 V (Figure 1c and d). The clear dependence of I_S on the gate voltage provides the evidence of Andreev transport occurring through the Ge QW. We expect the critical current I_C to be almost equal to the experimentally measured I_S as the Josephson energy $E_J \approx \frac{\hbar I_S}{2e} \approx k_B(2-25\,\mathrm{K})$ (k_B is the Boltzmann constant) is notably higher than the sample temperature, for the measured gate voltage range [23]. We further extract the characteristic $I_C R_N$ product reaching up to 360 µV in Figure 1e. In the Supplementary Figure S5, we find the $I_C R_N$ product for the same fabrication process with Al as the sole superconductor reaching values up to 50 µV indicating a superior interface achieved between Ge and Al with our fabrication process compared to earlier works [20, 24]. Harnessing the high quality S-Sm interface, we enhance the superconducting properties of Al, and the hybrid devices, by contacting the Al layer directly with Nb [25]. Therefore, we attribute the large $I_C R_N$ product to the combination of enhancement of the superconducting gap of Al due to contact with Nb and transparent Al-Ge interfaces.

Multiple Andreev Reflections (MARs) appearing at finite voltages further allow us to characterize the hybrid devices. They are subgap features occurring as resistance peaks for transparent S-Sm junctions at energies $eV = \frac{2\Delta_{el}}{n}$, where n is the number of times a quasiparticle is successively Andreev reflected and Δ_{el} is the

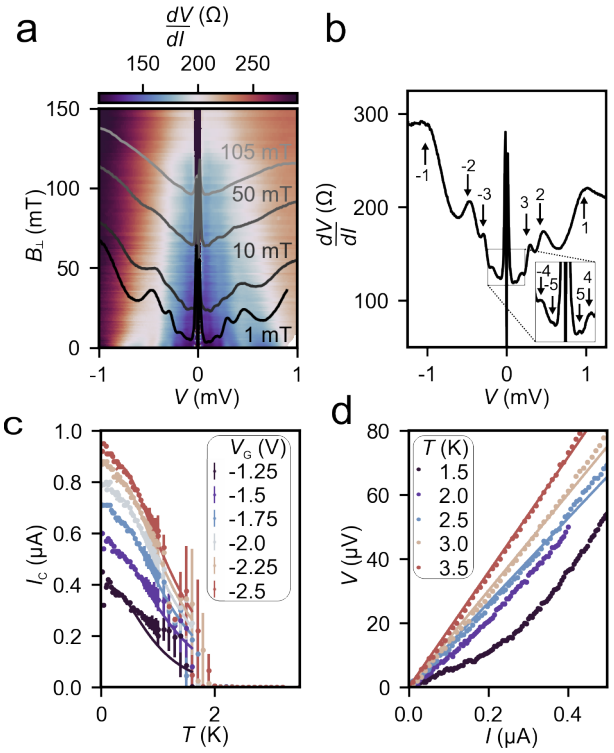

FIG. 2: **(a)** $\frac{dV}{dI}$ versus $B_\perp$ and V highlighting the presence of MAR. The overlying line traces show the evolution of MAR features with $B_\perp$. **(b)** $\frac{dV}{dI}$ versus V line trace from **(a)** showing the various orders of MAR peaks observed at $B_\perp = 0\,\mathrm{mT}$. The inset shows the higher order MAR features observed at lower values of V. **(c)** Temperature dependence of I_C for various V_G. The fitting of I_C to $\sqrt{T}\exp(-2\pi k_\mathrm{B}T/E_\mathrm{Th})$ allows to determine E_Th. **(d)** V-I characteristics of the JoFET showing increasing linearity at higher temperatures.

superconducting gap of the electrodes [26, 27]. We observe multiple orders of MAR indicating a high probability of Andreev reflection and large mean free paths in the JoFETs. From the zero magnetic field trace in Figure 2a, we deduce $\Delta_\mathrm{el} \approx 486\,\mu\mathrm{eV}$, markedly higher than that of bare Al ($\approx 180\,\mu\mathrm{eV}$) but lower than that of bare Nb ($\approx 1.5\,\mathrm{meV}$) providing further evidence of enlargement of Al's gap due to proximity with Nb [28]. At very low voltages in Figure 2b, we are able to explicitly observe MARs up to 5^th order putting a lower bound on the inelastic scattering length $l_\phi > 5L = 750\,\mathrm{nm}$. On an application of a perpendicular magnetic field, the MAR peaks evolve to lower voltage bias indicating the decay of the superconducting gap due to the magnetic field [29].

The variation of I_S with temperature allows us to determine different energy scales of the JoFET. We extract the Thouless energy E_Th by fitting the relation $I_\mathrm{C} \propto \sqrt{T}\exp(-2\pi k_\mathrm{B}T/E_\mathrm{Th})$ for different top gate voltages [30]. E_Th values obtained from the fits range from $295\,\mu\mathrm{eV}$ at $V_\mathrm{G} = -1.25\,\mathrm{V}$ to $370\,\mu\mathrm{eV}$ at $V_\mathrm{G} = -2.5\,\mathrm{V}$ in Figure 2c. Using the extracted values of E_Th, we estimate the superconducting coherence length $\xi_\mathrm{N} = \sqrt{\frac{E_\mathrm{Th}L^2}{\Delta_\mathrm{el}}}$ which falls in the range between 120 nm and 135 nm for the respective gate voltages. As expected, the supercurrent diminishes with increasing temperature due to the decrease of the superconducting gap of the electrodes. In Figure 2d, we find the non-linearity of the current-voltage (I-V) characteristics decreasing as the temperature increases and observe an almost linear IV curve at a critical temperature $T_\mathrm{C} \approx 3\,\mathrm{K}$. We extract a superconducting gap $\Delta_\mathrm{el} = 1.76 k_\mathrm{B}T_\mathrm{C} \approx 470\,\mu\mathrm{eV}$ which is in close agreement with the superconducting gap extracted from the analysis of MAR.

Comparing the superconducting gap with the extracted energy scales gives further insight into the regime of operation of the JoFETs. In the Supplementary Figure S7, we extract the excess current (I_excess) and find the ratio $\frac{eI_\mathrm{excess}R_\mathrm{N}}{\Delta_\mathrm{el}}$ to be 1.9, which is closer to the expected ratio for the ballistic regime ($\frac{8}{3}$) than that for the diffusive regime ($\frac{\pi^2}{4} - 1$) [31, 32]. The $I_\mathrm{excess}R_\mathrm{N}$ product also allows us to infer the S-Sm interface transparency using the Octavio-Blonder-Tinkham-Klapwijk (OBTK) model [33, 34]. We estimate a transparency of 90 % for our devices, a considerable improvement for the hybrid planar Ge platform. Furthermore, we find the $I_\mathrm{C}R_\mathrm{N}$ product to be $0.75\frac{\Delta_\mathrm{el}}{e}$ deviating from the theoretically expected $I_\mathrm{C}R_\mathrm{N} = 2\frac{\Delta_\mathrm{el}}{e}$ for the clean junctions [35]. As noted earlier, the longer channel length due to the etching procedure could result into the long junction regime ($l > \xi_\mathrm{N}$), decreasing the value of $I_\mathrm{C}R_\mathrm{N}$ [36].

B. Magnetic Field Behaviour

We now turn our attention to the magnetic field behavior of the JoFET devices. In the presence of a magnetic field oriented perpendicular to the substrate plane, a clear Fraunhofer modulation of the switching current is observed confirming the coupling between the two superconducting leads through Andreev transport (Figure 3a). The symmetry of the Fraunhofer pattern for positive and negative values of $B_\perp$ indicates the low disorder achieved with our fabrication procedure [37]. Based on the lithographic dimensions of the junction, a magnetic field of 6.9 mT should correspond to one magnetic flux quantum $\frac{h}{2e}$ threading through the junction area. From the Fraunhofer pattern, we extract a magnetic field of 0.8 mT, almost 9 times less than expected. We attribute this difference due to the flux focusing of the applied magnetic field caused by the Meissner effect [38]. By increasing the magnetic field to higher values in Figure 3b, we find the critical perpendicular magnetic field $B_{\perp,\mathrm{C}} = 460\,\mathrm{mT}$ for which the supercurrent vanishes. The parallel critical magnetic field $B_{\parallel,\mathrm{C}} = 1.8\,\mathrm{T}$ (Figure 3c) is almost 4 times higher as the thickness of the superconducting electrodes is much smaller than their width. The observed high magnetic field resilience paves the way for exploring the interplay of magnetic effects in Ge with induced super-

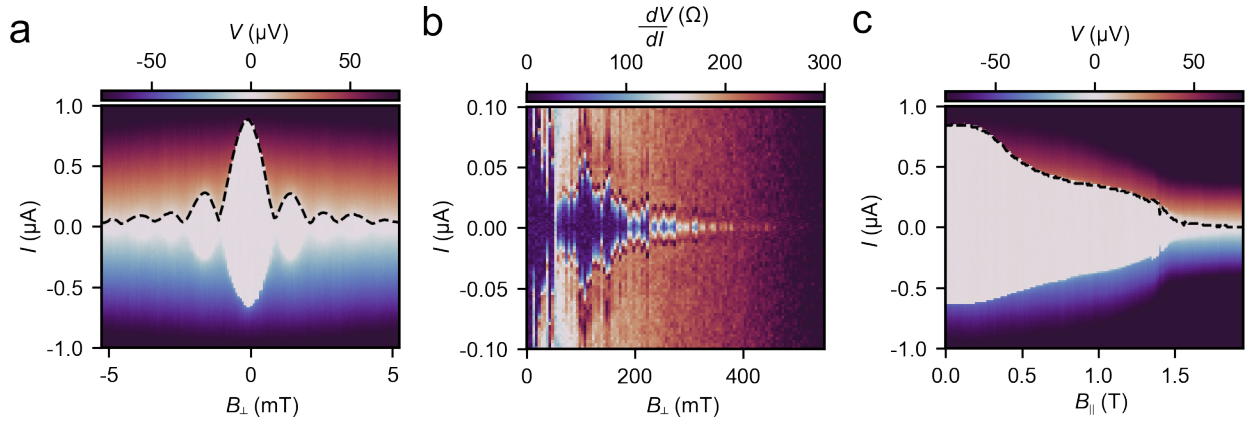

FIG. 3: **(a)** Color map of V across the JoFET versus $B_\perp$ and I showing the Fraunhofer pattern. The black dashed line is a guide to the eye highlighting the transition between the superconducting and normal state. **(b)** Differential resistance, $\frac{dV}{dI}$ versus $B_\perp$ and I showing the critical magnetic field and the overlying Fraunhofer pattern. **(c)** V versus $B_\parallel$ and I demonstrating that the critical current (black guideline) vanishes beyond 1.8 T.

conductivity and integration of disparate qubits such as spin qubits and gatemons on the same chip.

C. SQUID and CPR

Combining these high transparency junctions, we next explore the interference patterns arising through the control of the superconducting phase difference using a perpendicular magnetic field. Figure 4a shows an asymmetric SQUID combining JoFETs of 150 nm (JoFET 1) and 350 nm (JoFET 2) channel length with critical currents I_{C1} and I_{C2}, respectively. The asymmetric channel lengths and individual gate voltages allow biasing the two JoFETs in various regimes, ranging from a conventional SQUID to a superconducting phase control device.

We investigate the operation in a four-probe configuration, by applying a current and measuring the voltage difference between the SQUID arms under the application of a perpendicular magnetic field. The behavior of each of the individual junctions in the asymmetric SQUID can be found in the Supplementary Figure S9. When both top gate voltages are tuned to achieve the same critical current in each junction, we observe periodic oscillations of the critical current reflecting the underlying modulation of the superconducting phase due to a perpendicular magnetic field (Figure 4b). The modulation period of the oscillations $\Delta B \approx 370\,\mu$T corresponds to a magnetic flux quantum through an area of 5.5 μm^2 different from the lithographically defined area of the superconducting ring 1.8 μm^2. This difference can be attributed to the significant flux focusing due to the Meissner effect and the different resultant area due to the penetration depth, as already discussed before.

Tuning the ratio of the critical currents, allows phase-biasing the individual JoFET with the lower critical current. This allows to measure the current-phase relationship (CPR) which provides information about the underlying interfaces and physical phenomena at play [39–42]. In Figure 4c, JoFET 1 and JoFET 2 are biased using respective top gate voltages such that $\frac{I_{C1}}{I_{C2}} \approx 9$. In this limit, the change in the superconducting phase difference due to the magnetic field can be assumed to drop mainly over JoFET 2. The supercurrent in S-Sm-S JoFETs is carried by Andreev Bound States, due to which the CPR can be significantly different from a sinusoidal CPR expected for superconductor-insulator-superconductor (SIS) junctions [43]. We observe a particularly skewed CPR characteristic of a highly transparent S-N interface. We fit the relation $I(\phi) = I_C \frac{\sin\phi}{\sqrt{1-T\sin^2\phi}}$, taking into account the change of critical currents of the individual JoFETs due to Fraunhofer modulation, to extract the transparencies of our Nb-Al-Ge QW-Al-Nb junctions. It should be noted that this expression is derived for a single ballistic channel, however allows to extract the average transparency over many conduction channels as is the case for our 2D geometry [39, 41]. In Figure 4d, we find a transparency of 88±5 % concurrent with the excess current measurements.

III. CONCLUSION

In summary, our work provides evidence of highly transparent coupling between a superconductor and holes in a Ge QW. We find through $I_{\text{excess}}R_N$ measurements signatures of a ballistic weak link and low OBTK barrier strengths indicating high probability of Andreev reflection. The large observed values of $I_C R_N$, limited by the long junction regime, further confirms the quality of our interfaces. In addition, the gate tunability of the supercurrent and the clear Fraunhofer modulation demonstrates Andreev transport through the underlying semiconducting weak link. The ability to phase-bias individ-

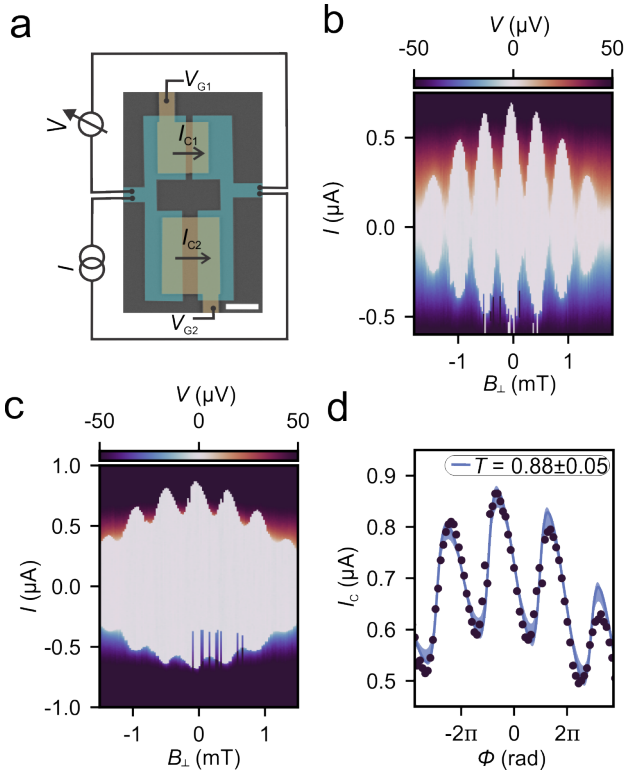

FIG. 4: **(a)** False-colored SEM image of an asymmetric SQUID with channel lengths of 150 nm and 350 nm and critical currents I_{C1} and I_{C2}, respectively. The scale bar is 1 µm. **(b)** SQUID oscillations of the I_C with $B_\perp$ at V_{G1} =−1.245 V and V_{G2} =−9 V.**(c)** Current-phase relationship of JoFET 2 with V_{G1} = −8 V and V_{G2} = −1.4 V such that the superconducting phase drops mainly over JoFET2. **(d)** I_C versus ϕ as extracted from **(c)**. Fitting the relation $I(\phi) = I_C \frac{\sin\phi}{\sqrt{1-T\sin^2\phi}}$ allows to extract transparencies of the S-Sm interface. The shaded region indicates an error of 5 % in the estimated transparency.

ual JJs will allow to investigate different proposals for Majorana physics. Furthermore, the indirect enhancement of induced superconductivity using the combination of Nb-Al can be extended to other material systems taking advantage of the ease of fabrication with Al and its large coherence length while making it more resilient to pair-breaking effects. Our developed system thus establishes Ge as a viable platform for exploring exotic phases and as a hybrid qubit platform for bringing together spin and superconducting qubits on the same chip.

Acknowledgments

This research and related results were made possible with the support of the NOMIS Foundation. This research was supported by the Scientific Service Units of IST Austria through resources provided by the MIBA Machine Shop and the nanofabrication facility, the European Union's Horizon 2020 research and innovation program under the Marie Sklodowska-Curie grant agreement #844511 and the Grant Agreement #862046. ICN2 acknowledge funding from Generalitat de Catalunya 2017 SGR 327. ICN2 is supported by the Severo Ochoa program from Spanish MINECO (Grant No. SEV-2017-0706) and is funded by the CERCA Programme / Generalitat de Catalunya. Part of the present work has been performed in the framework of Universitat Autònoma de Barcelona Materials Science PhD program. The HAADF-STEM microscopy was conducted in the Laboratorio de Microscopias Avanzadas at Instituto de Nanociencia de Aragon-Universidad de Zaragoza. Authors acknowledge the LMA-INA for offering access to their instruments and expertise. We acknowledge support from CSIC Research Platform on Quantum Technologies PTI-001. This project has received funding from the European Union's Horizon 2020 research and innovation programme under grant agreement No 823717 – ESTEEM3. M.B. acknowledges support from SUR Generalitat de Catalunya and the EU Social Fund; project ref. 2020 FI 00103. GS and MV acknowledge support through a projectruimte grant associated with the Netherlands Organization of Scientific Research (NWO).

DATA AVAILABILITY All transport data included in this work will be available on the IST Austria repository.

Appendix A: Methods

The 16 nm Ge QW heterostructure was grown by reduced chemical vapor deposition. Further details on the growth procedure can be found in Ref. [22]. The devices are fabricated using a 100 keV ebeam lithography system. First, a reactive ion plasma etching step, based on SF_6-O_2-CHF_3, is used to define mesa structures of ≈60 nm depth. This is followed by the deposition of the superconducting contacts. Before metal evaporation, the same plasma is used to etch ≈35 nm of the heterostructure to ensure a direct contact between the superconductor and the Ge QW. Then we clean the exposed Ge QW with a 10s BHF dip which is followed by a SF_6 plasma based passivation to reduce the contact resistance. A 15 nm thick layer of Al and a 30 nm thick layer of Nb forming the superconducting contacts is deposited. A ≈20nm thick layer of aluminium oxide is added at 150 °C by plasma atomic layer deposition, followed by a top-gate consisting of 3 nm Ti and 97 nm Pd.

We fabricated ten JoFETs, out of which two were not working due to leakage current through the gate oxide and the rest showed qualitatively similar supercurrents and $I_C R_N$ products.

[1] R. Aguado, Riv. Nuovo Cimento **40**, 523 (2017).

[2] R. M. Lutchyn, E. P. A. M. Bakkers, L. P. Kouwenhoven, P. Krogstrup, C. M. Marcus, and Y. Oreg, Nat. Rev. Mater. **3**, 52 (2018).

[3] J. Xiang, A. Vidan, M. Tinkham, R. M. Westervelt, and C. M. Lieber, Nature Nanotechnology **1**, 208 (2006), ISSN 1748-3395, URL https://doi.org/10.1038/nnano.2006.140.

[4] E. J. H. Lee, X. Jiang, M. Houzet, R. Aguado, C. M. Lieber, and S. De Franceschi, Nat. Nanotechnol. **9**, 79 (2014).

[5] J. Ridderbos, M. Brauns, A. Li, E. P. A. M. Bakkers, A. Brinkman, W. G. van der Wiel, and F. A. Zwanenburg, Phys. Rev. Materials **3**, 084803 (2019), URL https://link.aps.org/doi/10.1103/PhysRevMaterials.3.084803.

[6] C. Jünger, R. Delagrange, D. Chevallier, S. Lehmann, K. A. Dick, C. Thelander, J. Klinovaja, D. Loss, A. Baumgartner, and C. Schönenberger, Phys. Rev. Lett. **125**, 017701 (2020).

[7] L. Casparis, M. R. Connolly, M. Kjaergaard, N. J. Pearson, A. Kringhøj, T. W. Larsen, F. Kuemmeth, T. Wang, C. Thomas, S. Gronin, et al., Nature Nanotechnology **13**, 915 (2018), URL https://doi.org/10.1038/s41565-018-0207-y.

[8] T. W. Larsen, K. D. Petersson, F. Kuemmeth, T. S. Jespersen, P. Krogstrup, J. Nygård, and C. M. Marcus, Phys. Rev. Lett. **115**, 127001 (2015), URL https://link.aps.org/doi/10.1103/PhysRevLett.115.127001.

[9] T. W. Larsen, M. E. Gershenson, L. Casparis, A. Kringhøj, N. J. Pearson, R. P. G. McNeil, F. Kuemmeth, P. Krogstrup, K. D. Petersson, and C. M. Marcus, Phys. Rev. Lett. **125**, 056801 (2020), URL https://link.aps.org/doi/10.1103/PhysRevLett.125.056801.

[10] F. Luthi, T. Stavenga, O. W. Enzing, A. Bruno, C. Dickel, N. K. Langford, M. A. Rol, T. S. Jespersen, J. Nygård, P. Krogstrup, et al., Phys. Rev. Lett. **120**, 100502 (2018), URL https://link.aps.org/doi/10.1103/PhysRevLett.120.100502.

[11] K. D. Petersson, L. W. McFaul, M. D. Schroer, M. Jung, J. M. Taylor, A. A. Houck, and J. R. Petta, Nature **490**, 380 (2012), ISSN 1476-4687, URL https://doi.org/10.1038/nature11559.

[12] G. Burkard, M. J. Gullans, X. Mi, and J. R. Petta, Nature Reviews Physics **2**, 129 (2020).

[13] H. Watzinger, J. Kukučka, L. Vukušić, F. Gao, T. Wang, F. Schäffler, J.-J. Zhang, and G. Katsaros, Nature Communications **9** (2018).

[14] J. Ridderbos, M. Brauns, F. K. de Vries, J. Shen, A. Li, S. Kölling, M. A. Verheijen, A. Brinkman, W. G. van der Wiel, E. P. A. M. Bakkers, et al., Nano Letters **20**, 122 (2020), ISSN 1530-6984, URL https://doi.org/10.1021/acs.nanolett.9b03438.

[15] G. Scappucci, C. Kloeffel, F. A. Zwanenburg, D. Loss, M. Myronov, J.-J. Zhang, S. D. Franceschi, G. Katsaros, and M. Veldhorst, arXiv: 2004.08133 [cond-mat] (2020).

[16] N. W. Hendrickx, W. I. L. Lawrie, M. Russ, F. van Riggelen, S. L. de Snoo, R. N. Schouten, A. Sammak, G. Scappucci, and M. Veldhorst, arXiv: 2009.04268 [cond-mat] (2020).

[17] N. W. Hendrickx, D. P. Franke, A. Sammak, M. Kouwenhoven, D. Sabbagh, L. Yeoh, R. Li, M. L. V. Tagliaferri, M. Virgilio, G. Capellini, et al., Nature Communications **9** (2018).

[18] N. W. Hendrickx, M. L. V. Tagliaferri, M. Kouwenhoven, R. Li, D. P. Franke, A. Sammak, A. Brinkman, G. Scappucci, and M. Veldhorst, Phys. Rev. B **99**, 075435 (2019), URL https://link.aps.org/doi/10.1103/PhysRevB.99.075435.

[19] N. W. Hendrickx, D. P. Franke, A. Sammak, G. Scappucci, and M. Veldhorst, Nature **577**, 487 (2020).

[20] F. Vigneau, R. Mizokuchi, D. C. Zanuz, X. Huang, S. Tan, R. Maurand, S. Frolov, A. Sammak, G. Scappucci, F. Lefloch, et al., Nano Letters **19**, 1023 (2019), https://doi.org/10.1021/acs.nanolett.8b04275, URL https://doi.org/10.1021/acs.nanolett.8b04275.

[21] F. Pientka, A. Keselman, E. Berg, A. Yacoby, A. Stern, and B. I. Halperin, Phys. Rev. X **7**, 021032 (2017), URL https://link.aps.org/doi/10.1103/PhysRevX.7.021032.

[22] A. Sammak, D. Sabbagh, N. W. Hendrickx, M. Lodari, B. Paquelet Wuetz, A. Tosato, L. Yeoh, M. Bollani, M. Virgilio, M. A. Schubert, et al., Advanced Functional Materials **29**, 1807613 (2019), URL https://onlinelibrary.wiley.com/doi/abs/10.1002/adfm.201807613.

[23] M. Tinkham, *Introduction to Superconductivity* - (Courier Corporation, New York, 2004), ISBN 978-0-486-13472-7.

[24] N. W. Hendrickx, M. L. V. Tagliaferri, M. Kouwenhoven, R. Li, D. P. Franke, A. Sammak, A. Brinkman, G. Scappucci, and M. Veldhorst, Phys. Rev. B **99**, 075435 (2019), URL https://link.aps.org/doi/10.1103/PhysRevB.99.075435.

[25] M. G. Blamire, E. C. G. Kirk, J. E. Evetts, and T. M. Klapwijk, Phys. Rev. Lett. **66**, 220 (1991), URL https://link.aps.org/doi/10.1103/PhysRevLett.66.220.

[26] T. M. Klapwijk, G. E. Blonder, and M. Tinkham, Physica B **109 l& 110**, 1657*1664 (1982).

[27] D. Averin and A. Bardas, Phys. Rev. Lett. **75**, 1831 (1995), URL https://link.aps.org/doi/10.1103/PhysRevLett.75.1831.

[28] B. T. Matthias, T. H. Geballe, and V. B. Compton, Rev. Mod. Phys. **35**, 1 (1963), URL https://link.aps.org/doi/10.1103/RevModPhys.35.1.

[29] R. D. Parks, Journal of Applied Physics **39**, 2515 (1968).

[30] V. Z. Kresin, Phys. Rev. B **34**, 7587 (1986), URL https://link.aps.org/doi/10.1103/PhysRevB.34.7587.

[31] G. E. Blonder, M. Tinkham, and T. M. Klapwijk, Phys. Rev. B **25**, 4515 (1982), URL https://link.aps.org/doi/10.1103/PhysRevB.25.4515.

[32] S. Artemenko, A. Volkov, and A. Zaitsev, Solid State Communications **30**, 771 (1979), ISSN 0038-1098, URL http://www.sciencedirect.com/science/article/pii/0038109879900449.

[33] K. Flensberg, J. B. Hansen, and M. Octavio, Phys. Rev. B **38**, 8707 (1988), URL https://link.aps.org/doi/10.1103/PhysRevB.38.8707.

[34] M. Octavio, M. Tinkham, G. E. Blonder, and T. M. Klapwijk, Phys. Rev. B **27**, 6739 (1983), URL https://link.aps.org/doi/10.1103/PhysRevB.27.6739.

[35] I. O. Kulik and A. N. Omel'yanchuk, Sov. J. Low Temp.

Phys. **3:7** (1977).

[36] P. Dubos, H. Courtois, B. Pannetier, F. K. Wilhelm, A. D. Zaikin, and G. Schön, Phys. Rev. B **63**, 064502 (2001), URL https://link.aps.org/doi/10.1103/PhysRevB.63.064502.

[37] A. Rasmussen, J. Danon, H. Suominen, F. Nichele, M. Kjaergaard, and K. Flensberg, Phys. Rev. B **93**, 155406 (2016), URL https://link.aps.org/doi/10.1103/PhysRevB.93.155406.

[38] I. S. Khukhareva, Soviet Journal of Experimental and Theoretical Physics **16**, 828 (1963).

[39] F. Nichele, E. Portolés, A. Fornieri, A. M. Whiticar, A. C. C. Drachmann, S. Gronin, T. Wang, G. C. Gardner, C. Thomas, A. T. Hatke, et al., Phys. Rev. Lett. **124**, 226801 (2020), URL https://link.aps.org/doi/10.1103/PhysRevLett.124.226801.

[40] D. B. Szombati, S. Nadj-Perge, D. Car, S. R. Plissard, E. P. A. M. Bakkers, and L. P. Kouwenhoven, Nature Physics **12**, 568 (2016), URL https://doi.org/10.1038/nphys3742.

[41] W. Mayer, M. C. Dartiailh, J. Yuan, K. S. Wickramasinghe, E. Rossi, and J. Shabani, Nature Communications **11** (2020), URL https://doi.org/10.1038/s41467-019-14094-1.

[42] A. Assouline, C. Feuillet-Palma, N. Bergeal, T. Zhang, A. Mottaghizadeh, A. Zimmers, E. Lhuillier, M. Eddrie, P. Atkinson, M. Aprili, et al., Nature Communications **10** (2019), URL https://doi.org/10.1038/s41467-018-08022-y.

[43] A. A. Golubov, M. Y. Kupriyanov, and E. Il'ichev, Rev. Mod. Phys. **76**, 411 (2004), URL https://link.aps.org/doi/10.1103/RevModPhys.76.411.